Chinese Chemical Letters 32 (2021) 87–91

Contents lists available at ScienceDirect

Chinese Chemical Letters

journal homepage: www.elsevier.com/locate/cclet

Communication

Establishment of a new molecular model for mercury determination verified by single crystal X-ray diffraction, spectroscopic analysis and biological potentials

Jiapei Gu[a,b], Feifan Zhang[a], Ziman Zheng[a], Xiangqian Li[a,b], Runxuan Deng[a], Zhan Zhou[a,**], Lufang Ma[a], Wanqiang Liu[c], Qianming Wang[b,d,*]

[a] College of Chemistry and Chemical Engineering, Henan Key Laboratory of Function-Oriented Porous Materials, Luoyang Normal University, Luoyang 471934, China
[b] Key Laboratory of Theoretical Chemistry of Environment, Ministry of Education, School of Chemistry, South China Normal University, Guangzhou 510006, China
[c] School of Chemistry and Chemical Engineering, Hunan University of Science and Technology, Xiangtan 411201, China
[d] Guangdong Provincial Key Laboratory of Optical Information Materials and Technology & Institute of Electric Paper Displays, South China Academy of Advanced Optoelectronics, South China Normal University, Guangzhou 510006, China

ARTICLE INFO

Article history:
Received 20 July 2020
Received in revised form 11 August 2020
Accepted 15 September 2020
Available online 16 September 2020

Keywords:
Dicyanoisophorone
Ratiometric fluorescent probe
Mercury ions
Cell imaging
Zebrafish

ABSTRACT

A wide variety of molecular probes have been developed for real-time analysis, but most of organic fluorophores possess small Stokes shifts and self-absorption or inner filter effect that could not be avoided. In this study, a new dicyanoisophorone-based derivative (*E*)-*O*-(4-(2-(3-(dicyanomethylene)-5,5-dimethylcyclohex-1-en-1-yl)vinyl)phenyl)diphenylphosphinothioate (λ_{ex} = 405 nm, λ_{em} = 551 nm, denoted as ICM-S) with strong push-pull electron effect has been afforded and it exhibits red shift for absorption from 407 nm to 426 nm with distinct color change from pale yellow to deep yellow upon exposure to Hg^{2+}. Moreover, an easily distinguishable fluorescence color change follows the route from green, yellow to red in the presence of Hg^{2+} over the range of 0–90 μmol/L (detection limit = 137 nmol/L) can be observed by the naked eye under a UV lamp irradiation. Chlorodiphenylphosphine and sublimed-sulfur are incorporated as responsive sites and P-O bond has been cleaved upon the addition of mercury ions. During the recognition process, such dicyanoisophorone dye (ICM-S) has been evolved to 2-(3-(4-hydroxystyryl)-5,5-dimethylcyclohex-2-enylidene) malononitrile (ICM–OH). Clear evidences in the chemical processes can be identified *via* single crystal X-ray diffraction, spectroscopic analysis, photophysical studies and titration experiments. With the aim of exploring its potential in biological systems, its *in vitro* responses to Hg^{2+} have been evaluated in 293 T cells and the effectiveness in zebrafish model has also been verified.

As one of the most toxic heavy metal ions and widespread pollutants, mercury ion (Hg^{2+}) has caused serious adverse effects on both environment and human health [1–5]. The excessive toxicity of Hg^{2+} is derived from its high ability to bind with thiol groups in enzymes and proteins, which can be accumulated in organisms and may eventually lead to some diseases, such as heart disease, liver dysfunction, kidney failure, bone disease, breast cancer, prostatic cancer, nervous system damage and diabetes [6–11]. Currently, the Hg^{2+} level is widely used as a reliable indicator to diagnose these diseases [12–17]. Therefore, the development of targeted Hg^{2+} detection probes for safe evaluation under various physiological conditions will be urgently necessary.

Up to now, a few strategies have been used to detect Hg^{2+}, such as atomic spectroscopy, inductively coupled plasma mass spectroscopy (ICP-MS), surface-enhanced Raman scattering, cold vapor atomic fluorescence spectrometry, resonance Rayleigh scattering, colorimetric sensors, redox sensors, electrochemistry and fluorescence probe [18–27]. Among these methods, fluorescent information has been considered as an attractive and versatile tool due to its selectivity, high *in situ* sensitivity, and real-time, noninvasive or

* Corresponding author at: Key Laboratory of Theoretical Chemistry of Environment, Ministry of Education, School of Chemistry, South China Normal University, Guangzhou 510006, China.
** Corresponding author.
E-mail addresses: zhouzhan@lynu.edu.cn (Z. Zhou), qmwang@scnu.edu.cn (Q. Wang).

https://doi.org/10.1016/j.cclet.2020.09.021
1001-8417/

minimally invasive monitoring in living organisms. The light signal can provide rapid and spatiotemporal information on target analytes [28–36]. As a general concept, fluorescent probes based on "ratiometric response" behavior are preferable to either effects of fluorescence enhancement or quenching. Ratiometric fluorescent probes are defined as the relative changes of fluorescence intensities at two different wavelengths under same excitation wavelength. Such measurement is an efficient approach, which can improve the sensitivity and eliminate intensity fluctuations from instrumental or environmental factors [37–44]. Thus, the development of high selectivity ratiometric fluorescent probes for Hg^{2+} detection under various physiological conditions is required.

In this research, we have prepared a novel dicyanoisophorone-based ratiometric fluorescent probe ICM-S, which exhibited excellent selectivity, sensitivity and practicability for Hg^{2+} detection (Scheme S1 in Supporting information). The low detection limit (137 nmol/L) was calculated from the fluorescence titration results. ^{1}H NMR, HRMS studies and density functional theory (DFT) calculation demonstrated that Hg^{2+}-mediated cleavage of the thiophosphinate ester P-O bond in ICM-S and the transformation from ICM-S to ICM−OH was observed, resulting in significant changes in color and fluorescence. More importantly, living cells and zebrafish imaging experiments established the feasibility of this probe for the determination of Hg^{2+}. It has been expected this strategy may provide a promising chemical tool for tracking heavy metal ions in biological systems.

The proposed probe ICM-S was synthesized in three steps, as shown in Fig. S1 (Supporting information). Firstly, 2-(3,5,5-trimethylcyclohex-2-enylidene) malononitrile was obtained as white solid by the reaction of malononitrile with isophorone in absolute ethanol. Then, the reaction of 2-(3,5,5-trimethylcyclohex-2-enylidene) malononitrile with *p*-hydroxybenzaldehyde afforded the key intermediate ICM−OH as orange solid [24]. Finally, the probe ICM-S was synthesized as a yellow powder by the reaction of ICM−OH with Ph_2PCl and elemental sulfur in THF under nitrogen [4]. The chemical structure of probe ICM-S was well characterized by using ^{1}H NMR, HRMS and single crystal X-ray diffraction. For the crystallographic properties of ICM-S, the crystal structure was analyzed by Mercury software. Fig. 1 showed X-ray crystal structure and packing arrangement of ICM-S along the a-axis direction, the b-axis direction and the c-axis direction. The unit cell parameters ICM-S were given as $a = 9.1419$ Å, $b = 10.4376$ Å, $c = 15.9500$ Å, $\alpha = 91.253°$, $\beta = 95.210°$, $\gamma = 113.788°$, which has been assigned to the triclinic system. It can be seen that ICM-S possesses a good crystallization effect, the detailed crystal information was provided in Table S1 (Supporting information).

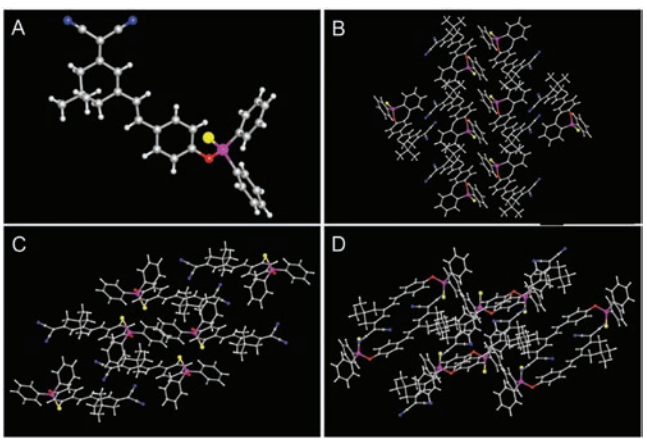

Fig. 1. X-ray crystal structure (A) and packing arrangement of ICM-S along the *a*-axis direction (B), the *b*-axis direction (C) and the *c*-axis direction (D). The C, N, O, P and S atoms were drawn in gray, blue, red, purple and yellow.

The spectral features and the response of probe ICM-S to Hg^{2+} were subsequently investigated under mild conditions. In this respect, response time is a key factor for a responsive probe. Therefore, the time dependent fluorescence responses of ICM-S toward Hg^{2+} (9.0 equiv.) were investigated. As shown in Fig. 2A, in the absence of Hg^{2+}, the emission band of ICM-S was located at 551 nm. Upon addition of Hg^{2+} and with increased incubation time, a dramatic enhancement in the emission at 582 nm was quickly detected, reached the maximum within 90 min, and then remained stable with increasing time (Fig. 2B). The result indicated that the fluorescence assay time of 90 min was selected in the evaluation of the selectivity and sensitivity of the ICM-S toward Hg^{2+} under mild conditions and without the assistance of any catalyst.

As shown in Fig. 2C, the fluorescent spectra of ICM-S in the absence or presence of Hg^{2+} at different concentrations were also explored. With the increasing concentration of Hg^{2+}, the fluorescence intensity at 582 nm was improved significantly. A good linear correlation ($R^2 = 0.9756$) of titration experiment was obtained and the detection limit (DL) was determined as 137 nmol/L through the equation DL = 3 × SD/slope, where SD is the standard deviation of the blank sample (Fig. 2D) [45,46]. Moreover, an easily distinguishable fluorescence color change from green, yellow to red with the increase of Hg^{2+} concentration can be observed by the naked eye under a UV lamp.

As a crucial parameter for assessing the properties of the probe in practical sensing, we investigated the selectivity of ICM-S toward various metal ions and common anions. Only the addition of Hg^{2+} to the probe solution caused obvious fluorescence intensity change at 551 nm and 582 nm (Figs. S2E and F in Supporting information). Therefore, ICM-S exhibited an outstanding selectivity toward Hg^{2+} among other common cations and anions (Fe^{3+}, Al^{3+}, Pb^{2+}, Ni^{2+}, Mg^{2+}, Cd^{2+}, Zn^{2+}, Na^+, K^+, Ag^+, HPO_4^{2-}, $H_2PO_4^-$, SO_4^{2-}, SO_3^{2-}, HSO_3^-, Cl^-, NO_3^-), which substantiated that the developed approach can be used for specific detection of Hg^{2+}.

Except the fluorometric titration, colorimetric sensing by naked eye is another efficient way to evaluate the selectivity of probe ICM-S. UV–vis absorption spectra observed before and after the addition of Hg^{2+} (0−90 μmol/L) to the solution of probe ICM-S (10 μmol/L) in DMSO-H_2O system (v/v, 1/1) were shown in Fig. S7 (Supporting information). Upon the addition of 9.0 equiv. of Hg^{2+} ions, ICM-S displayed a dramatic color change from pale yellow to deep yellow at room temperature. The absorption spectral experiments of ICM-S in the presence of various anions and cations were also performed. As shown in Fig. S8 (Supporting information), compared to other metal ions examined, only Hg^{2+} caused an obvious red-shift of the absorption of ICM-S from 407 nm to 426 nm, whereas no remarkable changes were found with other tested anions and cations. The selective visual color change can be used for the "naked eye" detection of Hg^{2+}.

To figure out the sensing mechanism of ICM-S to Hg^{2+}, fluorescence, UV–vis, ^{1}H NMR and HRMS spectra of ICM-S, ICM-S + Hg^{2+} and ICM−OH were performed. As shown in Fig. S9 (Supporting information), the UV–vis absorption spectrum of free ICM-S had an absorption band centered at 407 nm, which was attributed to the presence of the intramolecular charge transfer (ICT) in the conjugate system [28,39,47–49]. Upon the addition of Hg^{2+} (90 μmol/L), the maximum absorption peak at 407 nm was vanished, and a new absorption band appeared at around 426 nm which was nearly identical with the free ICM−OH. As shown in Fig. S10 (Supporting information), upon the addition of Hg^{2+} (90 μmol/L), the red band at 582 nm was significantly increased and the resultant emission curve was almost overlapped with the free ICM−OH. As shown in Fig. S11 (Supporting information), we carried out ^{1}H NMR experiments upon addition of Hg^{2+} to ICM-S in DMSO-d_6. With Hg^{2+} concentration was increased, the cleavage of

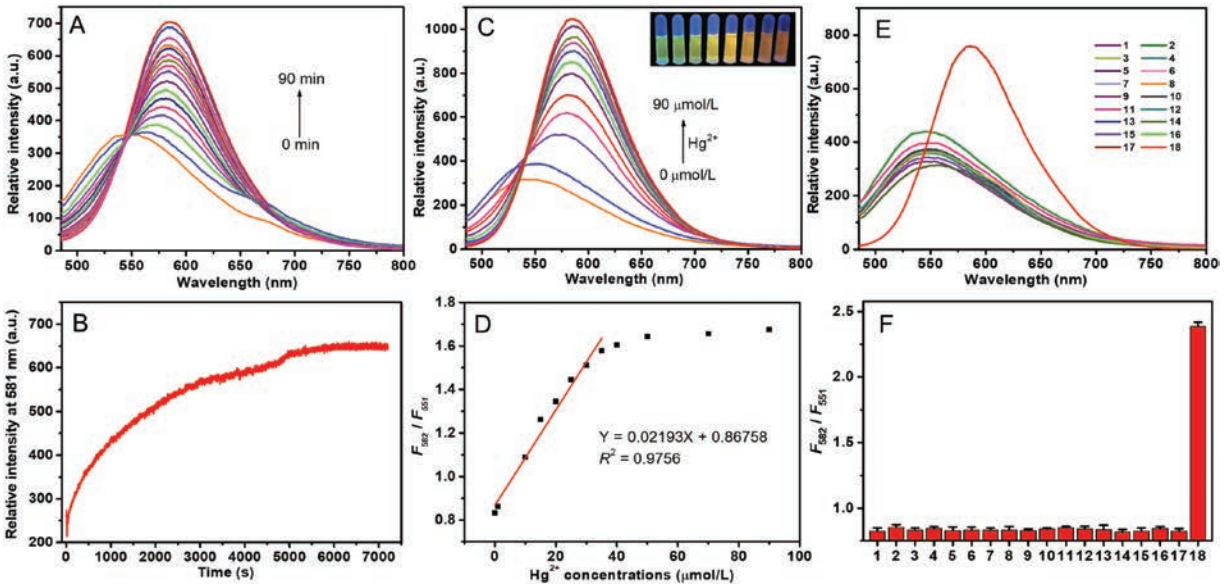

Fig. 2. (A) Time-dependent fluorescence emission spectra of ICM-S (10 μmol/L) with Hg^{2+} (90 μmol/L). (B) Time-dependent fluorescence intensity changes at 582 nm for solutions of ICM-S (10 μmol/L) upon addition of Hg^{2+} (90 μmol/L). (C) Fluorescence emission spectra of ICM-S (10 μmol/L) obtained upon addition of Hg^{2+} (0–90 μmol/L) in DMSO-H_2O system (v/v, 1/1) (inset: photograph of solutions of 10 μmol/L ICM-S upon addition of Hg^{2+} (0–90 μmol/L) under 365 nm hand-held UV lamp). (D) The changes of F_{582}/F_{551} of probe ICM-S (10 μmol/L) with the amount of Hg^{2+} (0–90 μmol/L). (E) Fluorescence emission spectra of probe ICM-S (10 μmol/L) before and after addition of 90 μmol/L different cations and anions (1. Fe^{3+}, 2. Al^{3+}, 3. Pb^{2+}, 4. Ni^{2+}, 5. Mg^{2+}, 6. Cd^{2+}, 7. Zn^{2+}, 8. Na^{+}, 9. K^{+}, 10. Ag^{+}, 11. HPO_4^{2-}, 12. $H_2PO_4^{-}$, 13. SO_4^{2-}, 14. SO_3^{2-}, 15. HSO_3^{-}, 16. Cl^{-}, 17. NO_3^{-}, 18. Hg^{2+}) in DMSO-H_2O system (v/v, 1/1). (F) Fluorescence intensity ratios (F_{582}/F_{551}) of probe ICM-S (10 μmol/L) before and after addition of 90 μmol/L different cations and anions (1. Fe^{3+}, 2. Al^{3+}, 3. Pb^{2+}, 4. Ni^{2+}, 5. Mg^{2+}, 6. Cd^{2+}, 7. Zn^{2+}, 8. Na^{+}, 9. K^{+}, 10. Ag^{+}, 11. HPO_4^{2-}, 12. $H_2PO_4^{-}$, 13. SO_4^{2-}, 14. SO_3^{2-}, 15. HSO_3^{-}, 16. Cl^{-}, 17. NO_3^{-}, 18. Hg^{2+}) in DMSO-H_2O system (v/v, 1/1).

the thiophosphinate ester P-O bond in ICM-S would occur [4]. It has been found that the proton peaks at 8.00, 7.97 ppm (Ha) and 7.61–7.58 ppm (Hb) assigned to the benzene attached to the phosphorus atoms were shifted to higher field strengths (7.74, 7.71 ppm (Ha') and 7.49–7.46 ppm (Hb')). At the same time, the new signals at 7.56, 7.25–7.18, 6.78 ppm were emerged which were consistent with the ^1H NMR data of ICM–OH. Moreover, the product of ICM-S + Hg^{2+} was further examined by HRMS, the achieved data *m/z* 289.1284 was attributed to ICM–OH $[M-H]^-$ (Fig. S12 in Supporting information). The reaction products of ICM-S with Hg^{2+} were isolated and utilized for standard characterization, which was unambiguously confirmed to be ICM–OH by X-ray single crystal structure (Fig. S6 and Table S2 in Supporting information). The above experimental results showed that ICM–OH and the mixture following reaction of ICM-S with Hg^{2+} were identical (Fig. S13 in Supporting information).

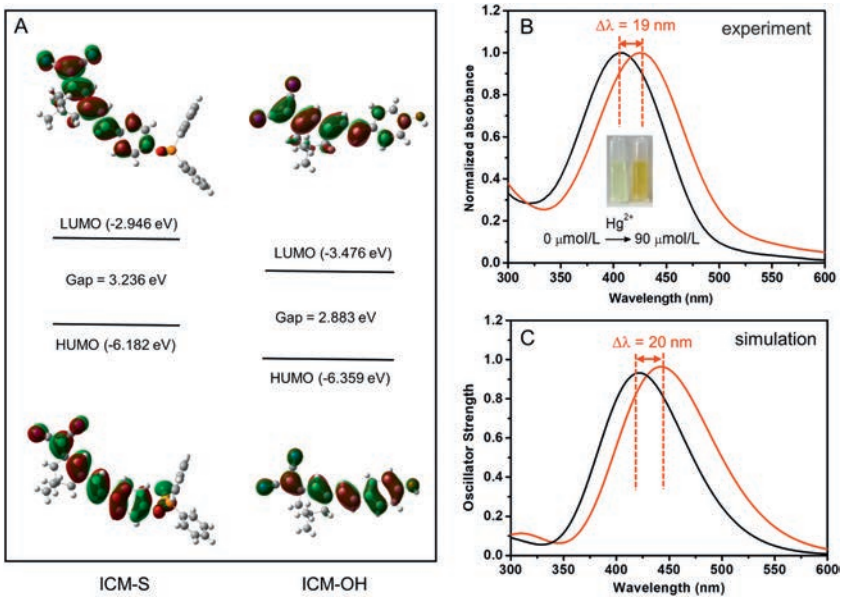

Fig. 3. (A) Frontier molecular orbital profiles of probe ICM-S and ICM–OH based on DFT (B3LYP/6-31G*) calculations. (B) The experimental UV–vis absorbance spectra of ICM-S (10 μmol/L) obtained upon addition of Hg^{2+} (0–90 μmol/L) in DMSO-H_2O system (v/v, 1/1) (inset: photograph of solutions of 10 μmol/L ICM-S before and after the addition of 90 μmol/L Hg^{2+} under day light) and (C) the simulated one.

The theoretical information about the molecular structure has been investigated and the Gaussian 09 program DFT calculations for ICM-S and ICM−OH were carried out at the level of B3LYP/6−31 G(d). As can be seen from Fig. 3A, the highest occupied molecular orbitals (HOMO) of ICM-S were dispersed in dicyanoisophorone unit and 4-hydroxystyryl group. The lowest unoccupied molecular orbitals (LUMO) were mainly localized on dicyanoisophorone unit and (vinylphenyl)phosphinothioate group, the results revealed an ICT character for ICM-S. In addition, release of thiophosphinate moiety in ICM-S afforded ICM−OH and such change triggered the decreasing of energy gap (ΔE) of ICM-S from 3.236 eV to 2.883 eV [25,50]. The absorption change of ICM-S in the presence of Hg^{2+} was also measured in Fig. 3B. In fact, upon addition of 9.0 equiv. of Hg^{2+} ions to the solution of robe ICM-S, the absorption band at 407 nm was slightly increased and a new band was formed at 426 nm, with a color change from pale yellow to deep yellow (Insert in Fig. 3B). As illustrated in Fig. 3C, the profile of the simulated absorption spectrum of ICM-S was exactly the same as the experimental curve. From a quantitative point of view, the computed data are in excellent agreement with the available experimental data for both absorption band position and relative intensity. In this way, the above DFT calculation supported the reliability of the red shift in the absorption spectrum (from 407 nm to 426 nm) of ICM-S with the treatment of Hg^{2+}.

The cytotoxicity studies for subsequent cellular imaging applications were evaluated. Probe ICM-S at different concentrations (0, 10, 20, 30, 40 and 50 μmol/L) and 293 T cells were incubated for 24 h in the medium. As shown in Fig. S14 (Supporting information), the survival rate of cells was above 90%, which indicated that ICM-S has good biocompatibility at low concentration to cells and can be used for biological imaging. The excellent Hg^{2+} sensing performance of ICM-S inspired us to evaluate its ability to detect Hg^{2+} in living cells. As given in Fig. S15A (Supporting information), 293 T cells stained by 10 μmol/L ICM-S alone showed weak fluorescence in the red channel. Upon addition of 30 μmol/L Hg^{2+}, the fluorescence intensity in the red channel was increased (Fig. S15B in Supporting information), this result provided evidence of good cell-membrane permeability of ICM-S. The fluorescent images shown in Fig. S15B clearly indicated that the intracellular fluorescence intensity exhibited an uneven distribution, which may be related to the distribution of Hg^{2+} in the cells. The fluorescence was significantly increased in the red channel at the higher concentration of 90 μmol/L Hg^{2+} (Fig. S15C in Supporting information). These results indicated ICM-S is able to penetrate into 293 T cells and could be used for the detection of Hg^{2+} in living cells.

The experiment of ICM-S applied for recognizing Hg^{2+} imaging in zebrafish was performed. In the first step, the zebrafish embryos were incubated at 28 °C with E3 medium containing ICM-S (10 μmol/L) for 2 h. Furthermore, the zebrafish embryos were further cultured with 30 and 90 μmol/L of Hg^{2+} for another 90 min, respectively. As described in Fig. 4, the fluorescence signal was observed in the green channel when zebrafish were treated with ICM-S without Hg^{2+} (Fig. 4A). In the presence of 30 μmol/L Hg^{2+} (Fig. 4B), the bright luminescence signals were collected in the red channel. The corresponding red emission was substantially enhanced at higher concentration of 90 μmol/L Hg^{2+} (Fig. 4C). These facts demonstrated that the probe ICM-S can be effective for Hg^{2+} imaging during *in vivo* studies.

In order to evaluate the feasibility of the ICM-S in real samples, we investigated the recoveries of Hg^{2+} using tap water samples from laboratory. The water samples were added with Hg^{2+} at different concentrations (5 μmol/L, 10 μmol/L and 20 μmol/L). As shown in Table S3 (Supporting information), Hg^{2+} was accurately determined in the spiked water samples, and the recovery rate of these samples is good (98.1%–103%).

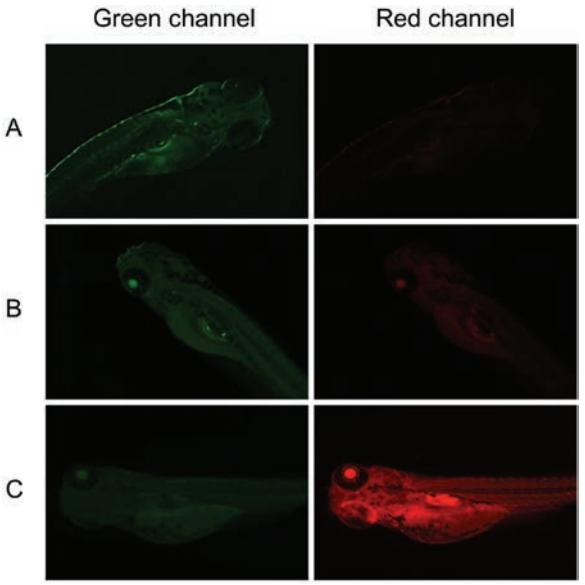

Fig. 4. Fluorescence microscope images of ICM-S (10 μmol/L) in zebrafish embryos. The zebrafish embryos were loaded with only ICM-S (10 μmol/L) as control (A) (green channel: λ_{ex} = 450–490 nm, λ_{em} = 512–542 nm). Embryos were further incubated with 30 μmol/L (B), or 90 μmol/L Hg^{2+} for 90 min (C) (red channel: λ_{ex} = 515–560 nm, λ_{em} = 590 nm).

The efficiency for most of optical probes was inherently limited by the spectral overlap between excitation and emission bands. In this contribution, the sensitive and selective detection of mercury ions has been realized *via* a dicyanoisophorone-based organic fluorophore. The recognition strategy was found to involve Hg^{2+} trigged cleavage of the thiophosphinate ester P-O bond in probe ICM-S to produce ICM−OH, which was fully characterized by ^{1}H NMR, HRMS analysis and DFT calculation. The probe ICM-S gave smart ratiometric response to only Hg^{2+} even in the presence of excessive amounts of other analytes. In addition, we have monitored the intracellular changes of Hg^{2+} in 293 T cells and such fluorescent signals can be resistant to interference within complicated cell culture medium. Further experiments explored its feasibility for tracking Hg^{2+} ions in zebrafish model. These new findings would facilitate the study of biological functions based on responsive molecular frameworks. It has to be mentioned that the stability of such organic fluorophore needs to be improved compared with inorganic/hybrid based sensor. Moreover, ICM-S was partially soluble in aqueous environment and the solubility might lead to slower response to guest ions. Additionally, the change from ICM-S to ICM−OH was not reversible in the presence of Hg^{2+} under current conditions. Future work will focus on the establishment of recyclable route during recognition process.

Declaration of competing interest

The authors report no declarations of interest.

Acknowledgments

Q. Wang thanks Guangzhou Science and Technology Plan (No. 202002030325), Science and Technology Plan of Guangdong Province (No. 2020A0505100055), National Natural Science Foundation of China-Guangdong Joint Funding Support (No. U1801256), Science and Technology Program of Guangzhou (No. 201905001) and Guangdong Provincial Key Laboratory of Optical Information Materials and Technology (No. 2017B030301007). L. Ma thanks Project of Central Plains Science and Technology

Innovation Leading Talents of Henan Province (No. 2042005 10001).

Appendix A. Supplementary data

Supplementary material related to this article can be found, in the online version, at doi:https://doi.org/10.1016/j.cclet.2020.09.021.

References

[1] J. Ding, H. Li, C. Wang, et al., ACS Appl. Mater. Interfaces 7 (2015) 11369–11376.
[2] Z. Ruan, L. Zong, Y. Song, et al., Sens. Actuators B: Chem. 226 (2016) 211–217.
[3] Y. Jiao, X. Liu, L. Zhou, et al., Sens. Actuators B: Chem. 247 (2017) 950–956.
[4] L. Chen, S.J. Park, D. Wu, H. Kim, J. Yoon Chem. Commun. 55 (2019) 1766–1769.
[5] T. Gao, X. Huang, S. Huang, et al., J. Agric. Food Chem. 67 (2019) 2377–2383.
[6] S.Y. Lin, H.J. Zhu, W.J. Xu, G. Wang, N. Fu, Chin. Chem. Lett. 25 (2014) 1291–1295.
[7] Y. Wang, H. Ding, S. Wang, et al., RSC Adv. 9 (2019) 11664–11669.
[8] S. Huang, T. Gao, A.Y. Bi, et al., Dyes Pigments 172 (2020) 107830.
[9] X. Wu, Y. Li, S. Yang, H. Tian, B. Sun, Dyes Pigments 174 (2020) 108056.
[10] Y. Yu, C. Liu, B. Tian, et al., Dyes Pigments 177 (2020) 108290.
[11] Z.X. Han, B.S. Zhu, T.L. Wu, et al., Chin. Chem. Lett. 25 (2014) 73–76.
[12] Y. Wang, M. Gao, C.Y. Liao, F. Yu, L. Chen, Sens. Actuators B: Chem. 301 (2019) 127038.
[13] S. Oh, J. Jeon, J. Jeong, et al., Anal. Chem. 92 (2020) 4917–4925.
[14] Y. Miao, X. Sun, J. Lv, G. Yan, Anal. Chem. 91 (2019) 5036–5042.
[15] X.D. Jiang, H.F. Yu, J.L. Zhao, et al., Chin. Chem. Lett. 26 (2015) 1241–1245.
[16] X. Li, G. Yuan, W. Yu, et al., Lab Chip 20 (2020) 414–423.
[17] Y. Liu, E.B. Yang, R. Han, et al., Chin. Chem. Lett. 25 (2014) 1065–1068.
[18] L. Li, Y. Feng, Y. Qiu, et al., Microchem. J. 155 (2020) 104762.
[19] S. Siddiqui, A. Nafady, H.M. El-Sagher, et al., J. Solid State Electr. 23 (2019) 2073–2083.
[20] Z. Zhou, X. Li, Y. Tang, et al., Chem. Eng. J. 351 (2018) 364–370.
[21] Z.Y. Li, Y.Y. Wang, M.N. Li, et al., Dyes Pigments 162 (2019) 339–347.
[22] H.Y. Li, H.Y. Lin, W.X. Lv, P. Gai, F. Li, Biosens. Bioelectron. 165 (2020) 112336.
[23] X. Li, Z. Zhou, Y. Tang, et al., Sens. Actuators B: Chem. 276 (2018) 95–100.
[24] M. Yang, J. Fan, W. Sun, et al., Chem. Commun. 55 (2019) 8583–8586.
[25] K. Wang, C.X. Zhao, T.H. Leng, et al., Dyes Pigments 151 (2018) 194–201.
[26] Z. Zhou, J. Gu, X. Qiao, et al., Sens. Actuators B: Chem. 282 (2019) 437–442.
[27] X. Qiu, X. Jiao, C. Liu, et al., Dyes Pigments 140 (2017) 212–221.
[28] S. Gong, J. Hong, E. Zhou, G.Q. Feng, Talanta 201 (2019) 40–45.
[29] X. Li, J. Gu, Z. Zhou, et al., Dyes Pigments 172 (2020) 107844.
[30] X. He, H. Chen, C. Xu, et al., J. Hazard. Mater. 388 (2020) 122029.
[31] P. Liu, N. Liu, C. Liu, et al., Dyes Pigments 163 (2019) 489–495.
[32] I. Ahmad, Z. Zhou, H.Y. Li, S.Q. Zang, Sens. Actuators B: Chem. 304 (2020) 127379.
[33] X. Li, Z. Zhou, C.C. Zhang, et al., Inorg. Chem. 57 (2018) 8866–8873.
[34] J.Y. Ren, P.S. Zhang, H. Liu, et al., Sens. Actuators B 304 (2020) 127299.
[35] X. He, W. Xiong, L.L. Zhang, et al., Dyes Pigments 174 (2020) 108059.
[36] Z. Zhou, J. Gu, Y. Chen, et al., Spectrochim. Acta Part A 212 (2019) 88–93.
[37] P. Zhang, H. Wang, Y. Hong, et al., Biosens. Bioelectron. 99 (2018) 318–324.
[38] X. He, Q. Xie, J. Fan, et al., Dyes Pigments 177 (2020) 108255.
[39] S. Wu, Y.J. Wei, Y.B. Wang, et al., Chin. Chem. Lett. 25 (2014) 93–98.
[40] J. Li, F. Huo, Z. Wen, C.X. Yin, Spectrochim. Acta Part A 221 (2019) 117156.
[41] Y. Yang, Y. Feng, Y.Z. Wang, et al., Sens. Actuators B: Chem. 253 (2017) 1055–1062.
[42] Y. Ding, Y. Pan, Y. Han, Ind. Eng. Chem. Res. 58 (2019) 7786–7793.
[43] L. Yang, Y. Su, Y. Geng, et al., Org. Biomol. Chem. 16 (2018) 5036–5042.
[44] C. Zhang, H. Zhang, M. Li, et al., Talanta 197 (2019) 218–224.
[45] L. Lan, Q. Niu, T. Li, Anal. Chim. Acta 1023 (2018) 105–114.
[46] B. Gu, L. Huang, W. Su, et al., Anal. Chim. Acta 954 (2017) 97–104.
[47] Y. Zhou, X. He, H. Chen, et al., Sens. Actuators B: Chem. 247 (2017) 626–631.
[48] G. Qiao, L. Liu, X. Hao, et al., Chem. Eng. J. 382 (2020) 122907.
[49] A. Yu, Y. Zhang, W. Liu, et al., Spectrochim. Acta A 233 (2020) 118218.
[50] X. Liu, X. Li, P. Dong, et al., Microchim. Acta 187 (2020) 313.